Hindawi Publishing Corporation
EURASIP Journal on Image and Video Processing
Volume 2008, Article ID 347050, 16 pages
doi:10.1155/2008/347050

*Research Article*

# Activity Representation Using 3D Shape Models

**Mohamed F. Abdelkader,[1] Amit K. Roy-Chowdhury,[2] Rama Chellappa,[1] and Umut Akdemir[3]**

[1] *Department of Electrical and Computer Engineering and Center for Automation Research, UMIACS, University of Maryland, College Park, MD 20742, USA*
[2] *Department of Electrical Engineering, University of California, Riverside, CA 92521, USA*
[3] *Siemens Corporate Research, Princeton, NJ 08540, USA*

Correspondence should be addressed to Mohamed F. Abdelkader, mdfarouk@umd.edu

Received 1 February 2007; Revised 9 July 2007; Accepted 25 November 2007

Recommended by Maja Pantic

We present a method for characterizing human activities using 3D deformable shape models. The motion trajectories of points extracted from objects involved in the activity are used to build models for each activity, and these models are used for classification and detection of unusual activities. The deformable models are learnt using the factorization theorem for nonrigid 3D models. We present a theory for characterizing the degree of deformation in the 3D models from a sequence of tracked observations. This degree, termed as deformation index (DI), is used as an input to the 3D model estimation process. We study the special case of ground plane activities in detail because of its importance in video surveillance applications. We present results of our activity modeling approach using videos of both high-resolution single individual activities and ground plane surveillance activities.



## 1. INTRODUCTION

Activity modeling and recognition from video is an important problem, with many applications in video surveillance and monitoring, human-computer interaction, computer graphics, and virtual reality. In many situations, the problem of activity modeling is associated with modeling a representative shape which contains significant information about the underlying activity. This can range from the shape of the silhouette of a person performing an action to the trajectory of the person or a part of his body. However, these shapes are often hard to model because of their deformability and variations under different camera viewing directions.

In all of these situations, shape theory provides powerful methods for representing these shapes [1, 2]. The work in this area is divided between 2D and 3D deformable shape representations. The 2D shape models focus on comparing the similarities between two or more 2D shapes [2–6]. Two-dimensional representations are usually computationally efficient and there exists a rich mathematical theory using which appropriate algorithms could be designed. Three-dimensional models have received much attention in the past few years. In addition to the higher accuracy provided by these methods, they have the advantage that they can potentially handle variations in camera viewpoint. However, the use of 3D shapes for activity recognition has been much less studied. In many of the 3D approaches, a 2D shape is represented by a finite-dimensional linear combination of 3D basis shapes and a camera projection model relating the 3D and 2D representations [7–10]. This method has been applied primarily to deformable object modeling and tracking. In [11], actions under different variability factors were modeled as a linear combination of spatiotemporal basis actions. The recognition in this case was performed using the angles between the action subspaces without explicitly recovering the 3D shape. However, this approach needs sufficient video sequences of the actions under different viewing directions and other forms of variability to learn the space of each action.

### 1.1. Major contributions of the paper

In this paper, we propose an approach for activity representation and recognition based on 3D shapes generated by the activity. We use the 3D deformable shape model for characterizing the objects corresponding to each activity. The underlying hypothesis is that an activity can be represented by deformable shape models that capture

the 3D configuration and dynamics of the set of points taking part in the activity. This approach is suitable for representing different activities as shown by experiments in Section 5. This idea has also been used for 2D shape-based representation in [12, 13]. We also propose a method for estimating the amount of deformation of a shape sequence by deriving a "deformability index" (DI). Estimation of the DI is noniterative, does not require selecting an arbitrary threshold, and can be done before estimating the 3D structure, which means that we can use it as an input to the 3D nonrigid model estimation process. We study the special case of ground plane activities in more detail as an important application because of its importance in surveillance scenarios. The 3D shapes in this special scenario are constrained by the ground plane which reduces the problem to a 2D shape representation. Our method in this case has the ability to match the trajectories across different camera viewpoints (which would not be possible using 2D shape modeling methods) and the ability to estimate the number of activities using the DI formulation. Preliminary versions of this work appeared in [14, 15] and a more detailed analysis of the concept of measuring the deformability was presented in [16].

We have tested our approach on different experimental datasets. First we validate our DI estimate using motion capture data as well as videos of different human activities. The results show that the DI is in accordance with our intuitive judgment and corroborates certain hypotheses prevailing in human movement analysis studies. Subsequently, we present the results of applying our algorithm to two different applications: view-invariant human activity recognition using 3D models (high-resolution imaging) and detection of anomalies in ground plane surveillance scenario (low-resolution imaging).

The paper is organized as follows. Section 2 reviews some of the existing work in event representation and 3D shape theory. Section 3 describes the shape-based activity modeling approach along with the special case of ground plane motion trajectories. Section 4 presents the method for estimating the DI for a shape sequence. Detailed experiments are presented in Section 5, before concluding in Section 6.

## 2. RELATED WORK

Activity representation and recognition have been an active area of research for decades and it is impossible to do justice to the various approaches within the scope of this paper. We outline some of the broad trends in this area. Most of the early work on activity representation comes from the field of artificial intelligence (AI) [17, 18]. More recent work comes from the fields of image understanding and visual surveillance, employing formalisms like hidden Markov models (HMMs), logic programming, and stochastic grammars [19–29]. A method for visual surveillance using a "forest of sensors" was proposed in [30]. Many uncertainty-reasoning models have been actively pursued in the AI and image understanding literature, including belief networks [31–33], Dempster-Shafer theory [34], dynamic Bayesian networks [35, 36], and Bayesian inference [37]. A specific area of research within the broad domain of activity recognition is human motion modeling and analysis, which has received keen interest from various disciplines [38–40]. A survey of some of the earlier methods used in vision for tracking human movement can be found in [41], while a more recent survey is in [42].

The use of shape analysis for activity and action recognition has been a recent trend in the literature. Kendall's statistical shape theory was used to model the interactions of a group of people and objects in [43], as well as the motion of individuals [44]. A method for the representation of human activities based on space curves of joint angles and torso location and attitude was proposed in [45]. In [46], the authors proposed an activity recognition algorithm using dynamic instants and intervals as view-invariant features, and the final matching of trajectories was conducted using a rank constraint on the 2D shapes. In [47], each human action was represented by a set of 3D curves which are quasi-invariant to the viewing direction. In [48, 49], the motion trajectories of an object are described as a sequence of flow vectors, and neural networks are used to learn the distribution of these sequences. In [50], a wavelet transform was used to decompose the raw trajectory into components of different scales, and the different subtrajectories are matched against a data base to recognize the activity.

In the domain of 3D shape representation, the approach of approximating a nonrigid object by a composition of basis shapes has been useful in certain problems related to object modeling [51]. However, there has been little analysis of its usefulness in activity modeling, which is the focus of this paper.

## 3. SHAPE-BASED ACTIVITY MODELS

### 3.1. Motivation

We propose a framework for recognizing activities by first extracting the trajectories of the various points taking part in the activity, followed by a nonrigid 3D shape model fitted to the trajectories. It is based on the empirical observation that many activities have an associated structure and a dynamical model. Consider, as an example, the set of images of a walking person in Figure 1(a) (obtained from the USF database for the gait challenge problem [52]). The binary representation clearly shows the change in the shape of the body for one complete walk cycle. The person in this figure is free to move his/her hands and feet any way he/she likes. However, this random movement does not constitute the activity of walking. For humans to perceive and appreciate the walk, the different parts of the body have to move in a certain synchronized manner. In mathematical terms, this is equivalent to modeling the walk by the deformations in the shape of the body of the person. Similar observations can be made for other activities performed by a single human, for example, dancing, jogging, sitting, and so forth.

An analogous example can be provided for an activity involving a group of people. Consider people getting off a plane and walking to the terminal, where there is no jet-bridge to constrain the path of the passengers (see


(a) (b)

Figure 1: Two examples of activities: (a) the binary silhouette of a walking person and (b) people disembarking from an airplane. It is clear that both of these activities can be represented by deformable shape models using the body contour in (a) and the passenger/vehicle motion paths in (b).

Figure 1(b)). Every person after disembarking is free to move as he/she likes. However, this does not constitute the activity of people getting off a plane and heading to the terminal. The activity here is comprised of people walking along a path that leads to the terminal. Again, we see that the activity can be modeled by the shape of the trajectories taken by the passengers. Using deformable shape models is a higher-level abstraction of the individual trajectories, and it provides a method of analyzing all the points of interest together, thus modeling their interactions in a very elegant way.

Not only is the activity represented by a deformable shape sequence, but also the amount of deformation is different for different activities. For example, it is reasonable to say that the shape of the human body while dancing is usually more deformable than during walking, which is more deformable than when standing still. Since it is possible for the human observer to roughly infer the degree of deformability based on the contents of the video sequence, the information about how deformable a shape is must be contained in the sequence itself. We will use this intuitive notion to quantify the deformability of a shape sequence from a set of tracked points on the object. In our activity representation model, a deformable shape is represented as a linear combination of rigid basis shapes [7]. The deformability index provides a theoretical framework for estimating the required number of basis shapes.

### 3.2. Estimation of deformable shape models

We hypothesize that each shape sequence can be represented by a linear combination of 3D basis shapes. Mathematically, if we consider the trajectories of $P$ points representing the shape (e.g., landmark points), then the overall configuration of the $P$ points is represented as a linear combination of the basis shapes $S_i$ as

$$S = \sum_{i=1}^{K} l_i S_i, \quad S, S_i \in \Re^{3\times P},\ l \in \Re, \tag{1}$$

where $l_i$ represents the weight associated with the basis shape $S_i$.

The choice of $K$ is determined by quantifying the deformability of the shape sequence, and it will be studied in detail in Section 4. We will assume a weak perspective projection model for the camera.

A number of methods exist in the computer vision literature for estimating the basis shapes. In the factorization paper for structure from motion [53], the authors considered $P$ points tracked across $F$ frames in order to obtain two $F \times P$ matrices, that is, $\mathbf{U}$ and $\mathbf{V}$. Each row of $\mathbf{U}$ contains the $x$-displacements of all the $P$ points for a specific time frame, and each row of $\mathbf{V}$ contains the corresponding $y$-displacements. It was shown in [53] that for 3D rigid motion and the orthographic camera model, the rank $r$ of the concatenation of the rows of the two matrices $[\mathbf{U}/\mathbf{V}]$ has an upper bound of 3. The rank constraint is derived from the fact that $[\mathbf{U}/\mathbf{V}]$ can be factored into two matrices, $\mathbf{M}_{2F\times r}$ and $\mathbf{S}_{r\times P}$, corresponding to the pose and 3D structure of the scene, respectively. In [7], it was shown that for nonrigid motion, the above method could be extended to obtain a similar rank constraint, but one that is higher than the bound for the rigid case. We will adopt the method suggested in [7] for computing the basis shapes for each activity. We will outline the basic steps of their approach in order to clarify the notation for the remainder of the paper.

Given $F$ frames of a video sequence with $P$ moving points, we first obtain the trajectories of all these points over the entire video sequence. These $P$ points can be represented in a measurement matrix as

$$\mathbf{W}_{2F\times P} = \begin{bmatrix} u_{1,1} & \cdots & u_{1,P} \\ v_{1,1} & \cdots & v_{1,P} \\ \vdots & \vdots & \vdots \\ u_{F,1} & \cdots & u_{F,P} \\ v_{F,1} & \cdots & v_{F,P} \end{bmatrix}, \tag{2}$$

where $u_{f,p}$ represents the $x$-position of the $p$th point in the $f$th frame and $v_{f,p}$ represents the $y$-position of the same point. Under weak perspective projection, the $P$ points of a configuration in a frame $f$ are projected onto 2D image points $(u_{f,i}, v_{f,i})$ as

$$\begin{bmatrix} u_{f,1} & \cdots & u_{f,P} \\ v_{f,1} & \cdots & v_{f,P} \end{bmatrix} = \mathbf{R}_f \left( \sum_{i=1}^{K} l_{f,i} S_i \right) + \mathbf{T}_f, \tag{3}$$

where

$$\mathbf{R}_f = \begin{bmatrix} r_{f1} & r_{f2} & r_{f3} \\ r_{f4} & r_{f5} & r_{f6} \end{bmatrix} \triangleq \begin{bmatrix} \mathbf{R}_f^{(1)} \\ \mathbf{R}_f^{(2)} \end{bmatrix}. \tag{4}$$

$\mathbf{R}_f$ represents the first two rows of the full 3D camera rotation matrix and $\mathbf{T}_f$ is the camera translation. The translation component can be eliminated by subtracting out the mean of all the 2D points, as in [53]. We now form the measurement matrix $\mathbf{W}$, which was represented in (2), with the means of each of the rows subtracted. The weak perspective scaling factor is implicitly coded in the configuration weights $\{l_{f,i}\}$.

Using (2) and (3), it is easy to show that

$$\mathbf{W} = \begin{bmatrix} l_{1,1}\mathbf{R}_1 & \cdots & l_{1,K}\mathbf{R}_1 \\ l_{2,1}\mathbf{R}_2 & \cdots & l_{2,K}\mathbf{R}_2 \\ \vdots & \vdots & \vdots \\ l_{F,1}\mathbf{R}_F & \cdots & l_{F,K}\mathbf{R}_F \end{bmatrix} \begin{bmatrix} S_1 \\ S_2 \\ \vdots \\ S_K \end{bmatrix} = \mathbf{Q}_{2F\times 3K} \cdot \mathbf{B}_{3K\times P}, \tag{5}$$

which is of rank $3K$. The matrix $\mathbf{Q}$ contains the pose for each frame of the video sequence and the weights $l_1, \ldots, l_K$. The matrix $\mathbf{B}$ contains the basis shapes corresponding to each of the activities. In [7], it was shown that $\mathbf{Q}$ and $\mathbf{B}$ can be obtained by using singular value decomposition (SVD) and retaining the top $3K$ singular values, as $\mathbf{W}_{2F\times P} = \mathbf{U}\mathbf{D}\mathbf{V}^T$ and $\mathbf{Q} = \mathbf{U}\mathbf{D}^{1/2}$ and $\mathbf{B} = \mathbf{D}^{1/2}\mathbf{V}^T$. The solution is unique up to an invertible transformation. Methods have been proposed for obtaining an invertible solution using the physical constraints of the problem. This has been dealt with in detail in previous papers [9, 51]. Although this is important for implementing the method, we will not dwell on it in detail in this paper and will refer the reader to previous work.

### 3.3. Special case: ground plane activities

A special case of activity modeling that often occurs is the case of ground plane activities, which are often encountered in applications such as visual surveillance. In these applications, the objects are far away from the camera such that each object can be considered as a point moving on a common plane such as the ground plane of the scene under consideration. Because of the importance of such configurations, we study them in more detail and present an approach for using our shape-based activity model to represent these ground plane activities. The 3D shapes in this case are reduced to 2D shapes due to the ground plane constraint. The main reason for using our 3D approach (as opposed to a 2D shape matching one) is the ability to match the trajectories across changes of viewpoint.

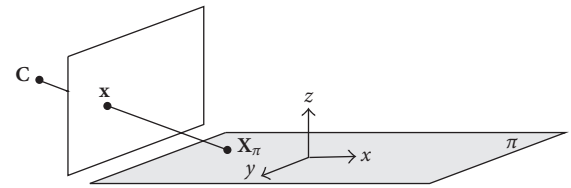


Figure 2: Perspective images of points in a plane [57]. The world coordinate system is moved in order to be aligned with the plane $\pi$.

Our approach for this situation consists of two steps. The first step recovers the ground plane geometry and uses it to remove the projection effects between the trajectories that correspond to the same activity. The second step uses the deformable shape-based activity modeling technique to learn a nominal trajectory that represents all the ground plane trajectories generated by an activity. Since each activity can be represented by one nominal trajectory, we will not need multiple basis shapes for each activity.

#### 3.3.1. First step: ground plane calibration

Most of the outdoor surveillance systems monitor a ground plane of an area of interest. This area could be the floor of a parking lot, the ground plane of an airport, or any other monitored area. Most of the objects being tracked and monitored are moving on this dominant plane. We use this fact to remove the camera projection effect by recovering the ground plane and projecting all the motion trajectories back onto this ground plane. In other words, we map the motion trajectories measured at the image plane onto the ground plane coordinates to remove these projective effects. Many automatic or semiautomatic methods are available to perform this calibration [54, 55]. As the calibration process needs to be performed only one time because the camera is fixed, we are using the semiautomatic method presented in [56], which is based on using some of the features often seen in man-made environments. We will give a brief summary of this method for completeness.

Consider the case of points lying on a world plane $\pi$, as shown in Figure 2. The mapping between points $\mathbf{X}_\pi = (X, Y, 1)^T$ on the world plane $\pi$ and their image $\mathbf{x}$ is a general planar homography—a plane-to-plane projective transformation—of the form $\mathbf{x} = H\mathbf{X}_\pi$, with $H$ being a $3 \times 3$ matrix of rank 3. This projective transformation can be decomposed into a chain of more specialized transformations of the form

$$H = H_S H_A H_P, \tag{6}$$

where $H_S$, $H_A$, and $H_P$ represent similarity, affine, and pure projective transformations, respectively. The recovery of the ground plane up to a similarity is performed in two stages.

*Stage 1: from projective to affine*

This is achieved by determining the pure projective transformation matrix $H_P$. We note that the inverse of this projective transformation is also a projective transformation $\hat{H}_P$, which can be written as

$$\hat{H}_P = \begin{bmatrix} 1 & 0 & 0 \\ 0 & 1 & 0 \\ l_1 & l_2 & l_3 \end{bmatrix}, \tag{7}$$

where $\mathbf{l}_\infty = (l_1, l_2, l_3)^T$ is the vanishing line of the plane, defined as the line connecting all the vanishing points for lines lying on the plane.

From (7), it is evident that identifying the vanishing line is enough to remove the pure projective part of the projection. In order to identify the vanishing line, two sets of parallel lines should be identified. Parallel lines are easy to find in man-made environments (e.g., parking space markers, curbs, and road lanes).

*Stage 2: from affine to metric*

The second stage of the rectification is the removal of the affine projection. As in the first stage, the inverse affine transformation matrix $\hat{H}_A$ can be written in the following form:

$$\hat{H}_A = \begin{bmatrix} \frac{1}{\beta} & -\frac{\alpha}{\beta} & 0 \\ 0 & 1 & 0 \\ 0 & 0 & 1 \end{bmatrix}. \tag{8}$$

Also, this matrix has two degrees of freedom represented by $\alpha$ and $\beta$. These two parameters have a geometric interpretation as representing the circular points, which are a pair of points at infinity that are invariant to Euclidean transformations. Once these points are identified, metric properties of the plane are available.

Identifying two affine invariant properties on the ground plane can be sufficient to obtain two constraints on the values of $\alpha$ and $\beta$. Each of these constraints is in the form of a circle. These properties include a known angle between two lines, equality of two unknown angles, and a known length ratio of two line segments.

### 3.3.2. Second step: learning trajectories

After recovering the ground plane (i.e., finding the projective $\hat{H}_P$ and affine $\hat{H}_A$ inverse transformations), the motion trajectories of the objects are reprojected to their ground plane coordinates. Having $m$ different trajectories of each activity, the goal is to obtain a nominal trajectory that represents all of these trajectories. We assume that all these trajectories have the same 2D shape up to a similarity transformation (translation, rotation, and scale). This transformation will compensate for the way the activity was performed in the scene. We use the factorization algorithm to obtain the shape of this nominal trajectory from all the motion trajectories.

For a certain activity that we wish to learn, let $T_j$ be the $j$th ground plane trajectory of this activity. This trajectory was obtained by tracking an object performing the activity in the image plane over $n$ frames and by projecting these points onto the ground plane as

$$T_j = \begin{bmatrix} x_{j1} & \cdots & x_{jn} \\ y_{j1} & \cdots & y_{jn} \\ 1 & \cdots & 1 \end{bmatrix} = \hat{H}_A \hat{H}_P \begin{bmatrix} u_{j1} & \cdots & u_{jn} \\ v_{j1} & \cdots & v_{jn} \\ 1 & \cdots & 1 \end{bmatrix}, \tag{9}$$

where $u, v$ are the 2D image plane coordinates, $x, y$ are the ground plane coordinates, and $\hat{H}_P$ and $\hat{H}_A$ are the pure projective and affine transformations from image to ground planes, respectively.

Assume, except for a noise term $\eta_j$, that all the different trajectories correspond to the same 2D nominal trajectory $S$ but have undergone 2D similarity transformations (scale, rotation, and translation). Then

$$\begin{aligned} T_j &= H_{Sj} S + \eta_j \\ &= \begin{bmatrix} s_j \cos\theta_j & -s_j \sin\theta_j & t_{xj} \\ s_j \sin\theta_j & s_j \cos\theta_j & t_{yj} \\ 0 & 0 & 1 \end{bmatrix} \begin{bmatrix} \tilde{x}_1 & \cdots & \tilde{x}_n \\ \tilde{y}_1 & \cdots & \tilde{y}_n \\ 1 & \cdots & 1 \end{bmatrix} + \eta_j, \end{aligned} \tag{10}$$

where $H_{Sj}$ is the similarity transformation between the $j$th trajectory and $S$. This relation can be rewritten in inhomogeneous coordinates as

$$\begin{aligned} \hat{T}_j &= \begin{bmatrix} s_j \cos\theta_j & -s_j \sin\theta_j \\ s_j \sin\theta_j & s_j \cos\theta_j \end{bmatrix} \begin{bmatrix} \tilde{x}_1 & \cdots & \tilde{x}_n \\ \tilde{y}_1 & \cdots & \tilde{y}_n \end{bmatrix} + \begin{bmatrix} t_{xj} \\ t_{yj} \end{bmatrix} + \eta_j \\ &= s_j R_j S + \mathbf{t}_j + \eta_j, \end{aligned} \tag{11}$$

where $s_j$, $R_j$, and $\mathbf{t}_j$ represent the scale, rotation matrix, and translation vector, respectively, between the $j$th trajectory and the nominal trajectory $S$.

In order to explore the temporal behavior of the activity trajectories, we divide each trajectory into small segments at different time scales and explore these segments. By applying this time scaling technique, which will be addressed in detail in Section 5, we obtain $m$ different trajectories, each with $n$ points. Given these trajectories, we can construct a measurement matrix of the form

$$W = \begin{bmatrix} \hat{T}_1 \\ \hat{T}_2 \\ \vdots \\ \hat{T}_m \end{bmatrix} = \begin{bmatrix} x_{11} & \cdots & x_{1n} \\ y_{11} & \cdots & y_{1n} \\ \vdots & & \vdots \\ x_{m1} & \cdots & x_{mn} \\ y_{m1} & \cdots & y_{mn} \end{bmatrix}_{2m \times n}. \tag{12}$$

As before, we subtract the mean of each row to remove the translation effect. Substituting from (11), the measurement matrix can be written as

$$W = \begin{bmatrix} s_1R_1 \\ s_2R_2 \\ \vdots \\ s_mR_m \end{bmatrix} S + \begin{bmatrix} \eta_1 \\ \eta_2 \\ \vdots \\ \eta_m \end{bmatrix} = P_{2m\times 2}S_{2\times n} + \eta. \tag{13}$$

Thus in the noiseless case, the measurement matrix has a maximum rank of two. The matrix $P$ contains the pose or orientation for each trajectory. The matrix $S$ contains the shape of the nominal trajectory for this activity.

Using the rank theorem for noisy measurements, the measurement matrix can be factorized into two matrices $\widetilde{P}$ and $\widetilde{S}$ by using SVD and retaining the top two singular values, as shown before:

$$W = UDV^T, \tag{14}$$

and taking $\widetilde{P} = U'D'^{1/2}$ and $\widetilde{S} = D'^{1/2}V'^T$, where $U', D', V'$ are the truncated versions of $U, D, V$ by retaining only the top two singular values. However, this factorization is not unique, as for any nonsingular $2 \times 2$ matrix $Q$,

$$W = \widetilde{P}\widetilde{S} = (\widetilde{P}Q)(Q^{-1}\widetilde{S}). \tag{15}$$

So we want to remove this ambiguity by finding the matrix $Q$ that would transform $\widetilde{P}$ and $\widetilde{S}$ into the pose and shape matrices $P = \widetilde{P}Q$ and $S = Q^{-1}\widetilde{S}$ as in (13). To find $Q$, we use the metric constraint on the rows of $P$, as suggested in [53].

By multiplying $P$ by its transpose $P^T$, we get

$$PP^T = \begin{bmatrix} s_1R_1 \\ \vdots \\ s_mR_m \end{bmatrix} \begin{bmatrix} s_1R_1 & \cdots & s_mR_m \end{bmatrix} = \begin{bmatrix} s_1^2\mathbf{I}_2 & & \\ & \ddots & \\ & & s_m^2\mathbf{I}_2 \end{bmatrix}, \tag{16}$$

where $\mathbf{I}_2$ is a $2 \times 2$ identity matrix. This follows from the orthonormality of the rotation matrices $R_j$. Substituting for $P = \widetilde{P}Q$, we get

$$PP^T = \widetilde{P}QQ^T\widetilde{P}^T = \begin{bmatrix} \mathbf{a_1} \\ \mathbf{b_1} \\ \vdots \\ \mathbf{a_m} \\ \mathbf{b_m} \end{bmatrix} QQ^T \begin{bmatrix} \mathbf{a_1}^T & \mathbf{b_1}^T & \cdots & \mathbf{a_m}^T & \mathbf{b_m}^T \end{bmatrix}, \tag{17}$$

where $\mathbf{a}_i$ and $\mathbf{b}_i$, $i = 1 : m$, are the odd and even rows of $\widetilde{P}$, respectively. From (16) and (17), we obtain the following constraints on the matrix $QQ^T$, for all $i = 1, \ldots, m$, such that

$$\begin{aligned} \mathbf{a}_iQQ^T\mathbf{a}_i^T &= \mathbf{b}_iQQ^T\mathbf{b}_i^T = s_i^2, \\ \mathbf{a}_iQQ^T\mathbf{b}_i^T &= 0. \end{aligned} \tag{18}$$

Using these $2m$ constraints on the elements of $QQ^T$, we can find the solution for $QQ^T$. Then $Q$ can be estimated through SVD, and it is unique up to a $2 \times 2$ rotation matrix. This ambiguity comes from the selection of the reference coordinate system and it can be eliminated by selecting the first trajectory as a reference, that is, by selecting $R_1 = I_{2\times 2}$.

#### 3.3.3. Testing trajectories

In order to test whether an observed trajectory $T_x$ belongs to a certain learnt activity or not, two steps are needed.

(1) Compute the optimal rotation and scaling matrix $s_xR_x$ in the least square sense such that

$$T_x \simeq s_xR_xS, \tag{19}$$

$$\begin{bmatrix} x_1 & \cdots & x_n \\ y_1 & \cdots & y_n \end{bmatrix} \simeq s_xR_x \begin{bmatrix} \widetilde{x}_1 & \cdots & \widetilde{x}_n \\ \widetilde{y}_1 & \cdots & \widetilde{y}_n \end{bmatrix}. \tag{20}$$

The matrix $s_xR_x$ has only two degrees of freedom, which correspond to the scale $s_x$ and rotation angle $\theta_x$; we can write the matrix $s_xR_x$ as

$$s_xR_x = \begin{bmatrix} s_x\cos\theta_x & -s_x\sin\theta_x \\ s_x\sin\theta_x & s_x\cos\theta_x \end{bmatrix}. \tag{21}$$

By rearranging (20), we get $2n$ equations in the two unknown elements of $s_xR_x$ in the form

$$\begin{bmatrix} x_1 \\ y_1 \\ \vdots \\ x_m \\ y_m \end{bmatrix} = \begin{bmatrix} \widetilde{x}_1 & -\widetilde{y}_1 \\ \widetilde{y}_1 & \widetilde{x}_1 \\ \vdots & \vdots \\ \widetilde{x}_m & -\widetilde{y}_m \\ \widetilde{y}_m & \widetilde{x}_m \end{bmatrix} \begin{bmatrix} s_x\cos\theta_x \\ s_x\sin\theta_x \end{bmatrix}. \tag{22}$$

Again, this set of equations is solved in the least square sense to find the optimal $s_xR_x$ parameters that minimize the mean square error between the tested trajectory and the rotated nominal shape for this activity.

(2) After the optimal transformation matrix is calculated, the correlation between the trajectory and the transformed nominal shape is calculated and used for making a decision. The Frobenius norm of the error matrix is used as an indication of the level of correlation, which represents the mean square error (MSE) between the two matrices. The error matrix is calculated as the difference between the tested trajectory matrix $T_x$ and the rotated activity shape as follows:

$$\Delta_x = T_x - s_xR_xS. \tag{23}$$

The Frobenius norm of a matrix $\mathbf{A}$ is defined as the square root of the sum of the absolute squares of its elements:

$$\|A\|_F = \sqrt{\sum_{i=1}^{m}\sum_{j=1}^{n} |a_{ij}^2|}. \tag{24}$$

The value of the error is normalized with the signal energy to give the final normalized mean square error (NMSE) defined as

$$\text{NMSE} = \frac{||\Delta_x||_F}{||T_x||_F + ||s_x R_x S||_F}. \quad (25)$$

Comparing the value of this NMSE to NMSE values of learnt activities, a decision can be made as to whether the observed trajectory belongs to this activity or not.

## 4. ESTIMATING THE DEFORMABILITY INDEX (DI)

In this section, we present a theoretical method for estimating the amount of deformation in a deformable 3D shape model. Our method is based on applying subspace analysis on the trajectories of the object points tracked over a video sequence. The estimation of DI is essential for our activity modeling approach that has been explained above. From one point of view, DI represents the amount of deformation in the 3D shape representing the activity. In other words, it represents the number of basis shapes ($k$ in (1)) needed to represent each activity. On the other hand, in the analysis of ground plane activities, the estimated DI can be used to estimate the number of activities in the scene (i.e., to find the number of nominal trajectories) as we assume that each activity can be represented by a single trajectory on the ground plane.

We will use the word trajectory to refer to either the tracks of a certain point of the object across different frames or to the trajectories generated by different objects moving in the scene in the ground plane scenario.

Consider each trajectory obtained from a particular video sequence to be the realization of a random process. Represent the $x$ and $y$ coordinates of the sampled points on these trajectories for one such realization as a vector $\mathbf{y} = [u_1, \ldots, u_P, v_1, \ldots, v_P]^T$. Then from (5), it is easy to show that for a particular example with $K$ distinct motion trajectories ($K$ is unknown),

$$\mathbf{y}^T = [l_1\mathbf{R}^{(1)}, \ldots, l_K\mathbf{R}^{(1)}, l_1\mathbf{R}^{(2)}, \ldots, l_K\mathbf{R}^{(2)}] * \begin{bmatrix} S_1 & \\ \vdots & 0 \\ S_k & \\ & S_1 \\ 0 & \vdots \\ & S_k \end{bmatrix} + \eta^T \quad (26)$$

that is,

$$\mathbf{y} = \left(\mathbf{q}_{1\times 6K}\mathbf{b}_{6K\times 2P}\right)^T + \eta = \mathbf{b}^T\mathbf{q}^T + \eta, \quad (27)$$

where $\eta$ is a zero-mean noise process. Let $\mathbf{R}_\mathbf{y} = E[\mathbf{y}\mathbf{y}^T]$ be the correlation matrix of $\mathbf{y}$ and let $\mathbf{C}_\eta$ be the covariance matrix of $\eta$. Hence

$$\mathbf{R}_\mathbf{y} = \mathbf{b}^T E[\mathbf{q}^T\mathbf{q}]\mathbf{b} + \mathbf{C}_\eta. \quad (28)$$

$\mathbf{C}_\eta$ represents the accuracy with which the feature points are tracked and can be estimated from the video sequence using the inverse of the Hessian matrix at each of the points. Since $\eta$ need not be an IID noise process, $\mathbf{C}_\eta$ will not necessarily have a diagonal structure (but it is symmetric). However, consider the singular value decomposition of $\mathbf{C}_\eta = \mathbf{P}\mathbf{\Lambda}\mathbf{P}^T$, where $\mathbf{\Lambda} = \text{diag}[\mathbf{\Lambda}_s, 0]$ and $\mathbf{\Lambda}_s$ is an $L\times L$ matrix of nonzero singular values of $\mathbf{\Lambda}$. Let $\mathbf{P}_s$ denote the columns of $\mathbf{P}$ corresponding to the nonzero singular values. Therefore, $\mathbf{C}_\eta = \mathbf{P}_s\mathbf{\Lambda}_s\mathbf{P}_s^T$. Premultiplying (27) by $\mathbf{\Lambda}_s^{-1/2}\mathbf{P}_s^T$, we see that (27) becomes

$$\widetilde{\mathbf{y}} = \widetilde{\mathbf{b}}^T\mathbf{q}^T + \widetilde{\eta}, \quad (29)$$

where $\widetilde{\mathbf{y}} = \mathbf{\Lambda}_s^{-1/2}\mathbf{P}_s^T\mathbf{y}$ is an $L\times 1$ vector, $\widetilde{\mathbf{b}} = \mathbf{\Lambda}_s^{-1/2}\mathbf{P}_s^T\mathbf{b}^T$ is an $L\times 6K$ matrix, and $\widetilde{\eta} = \mathbf{\Lambda}_s^{-1/2}\mathbf{P}_s^T\eta$. It can be easily verified that the covariance of $\widetilde{\eta}$ is an identity matrix $\mathbf{I}_{L\times L}$. This is known as the process of "whitening," whereby the noise process is transformed to be IID. Representing by $\mathbf{R}_{\widetilde{\mathbf{y}}}$ the correlation matrix of $\widetilde{\mathbf{y}}$, it is easy to see that

$$\mathbf{R}_{\widetilde{\mathbf{y}}} = \widetilde{\mathbf{b}}^T E[\mathbf{q}^T\mathbf{q}]\widetilde{\mathbf{b}} + \mathbf{I} = \mathbf{\Delta} + \mathbf{I}. \quad (30)$$

Now, $\mathbf{\Delta}$ is of rank $6K$, where $K$ is the number of activities. Representing by $\mu_i(\mathbf{A})$ the $i$th eigenvalue of the matrix $\mathbf{A}$, we see that $\mu_i(\widetilde{\mathbf{y}}) = \mu_i(\mathbf{\Delta}) + 1$ for $i = 1, \ldots, 6K$ and $\mu_i(\widetilde{\mathbf{y}}) = 1$ for $i = 6K+1, \ldots, L$. Hence, by comparing the eigenvalues of the observation and noise processes, it is possible to estimate the deformability index. This is done by counting the number of eigenvalues of $\mathbf{R}_{\widetilde{\mathbf{y}}}$ that are greater than 1, and dividing that number by 6 to get the DI value. The number of basis shapes can then be obtained by rounding the DI to the nearest integer.

### 4.1. Properties of the deformability index

(i) For the case of a 3D rigid body, the DI is 1. In this case, the only variation in the values of the vector $\mathbf{y}$ from one image frame to the next is due to the global rigid translation and rotation of the object. The rank of the matrix $\mathbf{\Delta}$ will be 6 and the deformability index will be 1.

(ii) Estimation of the DI does not require explicit computation of the 3D structure and motion in (5), as we need only to compute the eigenvalues of the covariance matrix of 2D feature positions. In fact, for estimating the shape and rotation matrices in (5), it is essential to know the value of $K$. Thus the method outlined in this section should precede computation of the shape in Section 3. Using our method, it is possible to obtain an algorithm for deformable shape estimation without having to guess the value of $K$.

(iii) The computation of the DI takes into account any rigid 3D translation and rotation of the object (as recoverable under a scaled orthographic camera projection model) even though it has the simplicity of working only with the covariance matrix of the 2D projections. Thus it is more general than a method that considers purely 2D image plane motion.

(iv) The "whitening" procedure described above enables us to choose a *fixed* threshold of one for comparing the eigenvalues.

Table 1: Deformability index (DI) for human activities using motion-capture data.

| | Activity | DI | | Activity | DI |
|---|---|---|---|---|---|
| (1) | Male walk (sequence 1) | 5.8 | (10) | Broom (sequence 2) | 8.8 |
| (2) | Male walk (sequence 2) | 4.7 | (11) | Jog | 5 |
| (3) | Fast walk | 8 | (12) | Blind walk | 8.8 |
| (4) | Walk throwing hands around | 6.8 | (13) | Crawl | 8 |
| (5) | Walk with drooping head | 8.8 | (14) | Jog while taking U-turn (sequence 1) | 4.8 |
| (6) | Sit (sequence 1) | 8 | (15) | Jog while taking U-turn (sequence 2) | 5 |
| (7) | Sit (sequence 2) | 8.2 | (16) | Broom in a circle | 9 |
| (8) | Sit (sequence 3) | 8.2 | (17) | Female walk | 7 |
| (9) | Broom (sequence 1) | 7.5 | (18) | Slow dance | 8 |

## 5. EXPERIMENTAL RESULTS

We performed two sets of experiments to show the effectiveness of our approach for characterizing activities. In the first set, we use 3D shape models to model and recognize the activities performed by an individual, for example, walking, running, sitting, crawling, and so forth. We show the effect of using a 3D model in recognizing these activities from different viewing angles. In the second set of experiments, we provide results for the special case of ground plane surveillance trajectories resulting from a motion detection and tracking system [58]. We explore the effectiveness of our formulation in modeling nominal trajectories and detecting anomalies in the scene. In the first experiment, we assume a robust tracking of the feature points across the sequence. This enables us to focus on whether the 3D models can be used to disambiguate between different activities in various poses and the selection of the criterion to make this decision. However, as pointed out in the original factorization paper [53] and in its extensions to deformable shape model in [7], the rank constraint algorithms can estimate the 3D structure even with noisy tracking results.

### 5.1. Application in human activity recognition

We used our approach to classify the various activities performed by an individual. We used the motion-capture data [59] available from Credo Interactive Inc. and Carnegie Mellon University in the BioVision Hierarchy and Acclaim formats. The combined dataset includes a number of subjects performing various activities like walking, jogging, sitting, crawling, brooming, and so forth. For each activity, we have multiple video sequences consisting of 72 frames each, acquired at different view points.

#### 5.1.1. Computing the DI for different human activities

For the different activities in the database, we used an articulated 3D model for the body that contains 53 tracked feature points. We used the method described in Section 4 on the trajectories of these points to compute the DI for each of these sequences. These values are shown in Table 1 for various activities. Please note that the DI is used to estimate the number of basis shapes needed for 3D deformable object modeling, not for activity recognition.

From Table 1, a number of interesting observations can be made. For the walk sequences, the DI is between 5 and 6. This matches the hypotheses in papers on gait recognition where it is mentioned that about five exemplars are necessary to represent a full cycle of gait [60]. The number of basis shapes increases for fast walk, as expected from some of the results in [61]. When the stick figure person walks doing some other things (like moving head or hands or a blind person's walk), the number of basis shapes needed to represent it (i.e., the deformability index) increases more than that of normal walk. The result that might seem surprising initially is the high DI for sitting sequences. On closer examination though, it can be seen that the stick figure, while sitting, is making all kinds of random gestures as if talking to someone else, increasing the DI for these sequences. Also, the DI is insensitive to changes in viewpoint (azimuth angle variation only), as can be seen by comparing the jog sequences (14 and 15 with 11) and broom sequences (16 with 9 and 10). This is not surprising since we do not expect the deformation of the human body to change due to rotation about the vertical axis. The DI, thus calculated, is used to estimate the 3D shapes, some of which are shown in Figure 3 and used in activity recognition experiments.

#### 5.1.2. Activity representation using 3D models

Using the video sequences and our knowledge of the DI for each activity, we applied the method outlined in Section 3 to compute the basis shapes and their combination coefficients (see (1)). The orthonormality constraints in [7] are used to get a unique solution for the basis shapes. We found that the first basis shape, $S_1$, contained most of the information. The estimated first basis shapes are shown in Figure 3 for six different activities. For this application, considering only the first basis shape was enough to distinguish between the different activities; that is, the recognition results did not improve with adding more basis shapes although the differences between the different models increased. This is a peculiarity of this dataset and will not be true in general. In order to compute the similarity measure, we considered the various joint angles between the different parts of the estimated 3D models. The angles considered are shown in

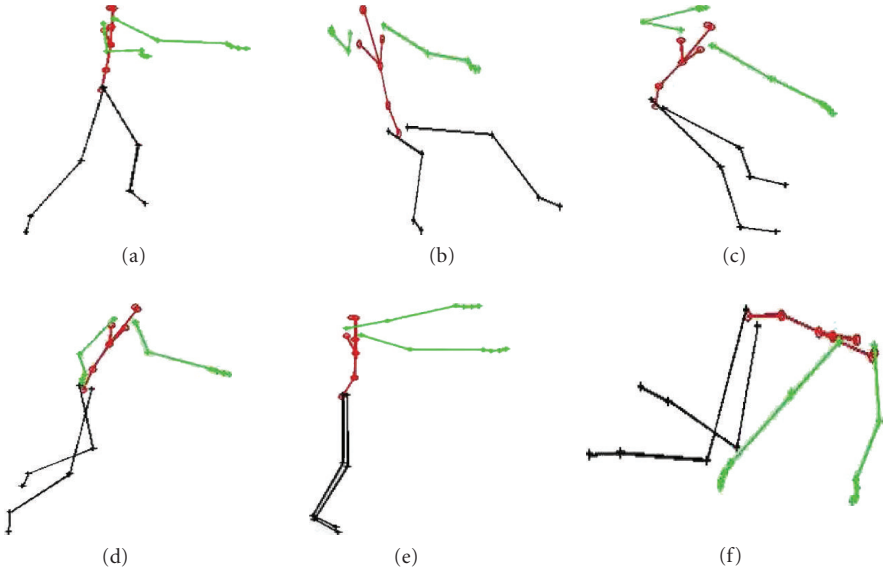


FIGURE 3: Plots of the first basis shap $S_1$ for (a)–(c) walk, sit, and broom sequences and for (d)–(f) jog, blind walk, and crawl sequences.

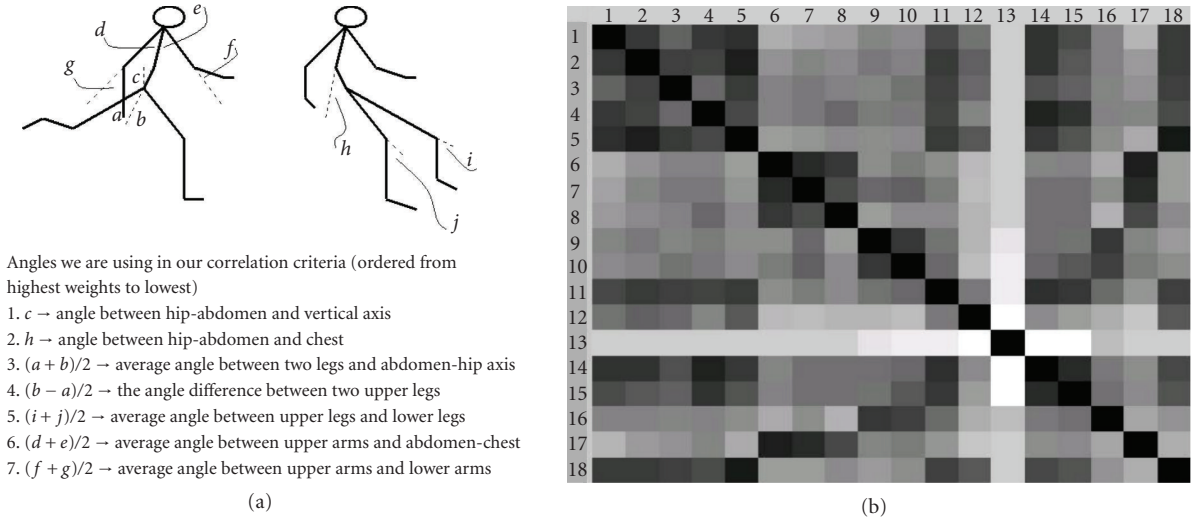


FIGURE 4: (a) The various angles used for computing the similarity of two models are shown in the figure. The text below describes the seven-dimensional vector computed from each model whose correlation determines the similarity scores. (b) The similarity matrix for the various activities, including ones with different viewing directions. The numbers correspond to the numbers in Table 1 for 1–16. 17 and 18 correspond to sitting and walking, where the training and test data are from two different viewing directions.

Figure 4(a). The idea of considering joint angles for activity modeling has been suggested before in [45]. We considered the seven-dimensional vector obtained from the angles as shown in Figure 4(a). The distance between the two angle vectors was used as a measure of similarity. Thus small differences indicate higher similarity.

The similarity matrix is shown in Figure 4(b). The row and column numbers correspond to the numbers in Table 1 for 1–16, while 17 and 18 correspond to sitting and walking, where the training and test data are from two different viewing directions. For the moment, consider the upper $13 \times 13$ block of this matrix. We find that the different walk sequences are close to each other; this is also true for sitting and brooming sequences. The jog sequence, besides being closest to itself, is also close to the walk sequences. Blind walk is close to jogging and walking. The crawl sequence does not match any of the rest and this is clear from row 13 of the matrix. Thus, the results obtained using our method are reasonably close to what we would expect from a human observer, which support the use of this representation in activity recognition.

In order to further show the effectiveness of this approach, we used the obtained similarity matrix to analyze the recognition rates for different clusters of activities. We

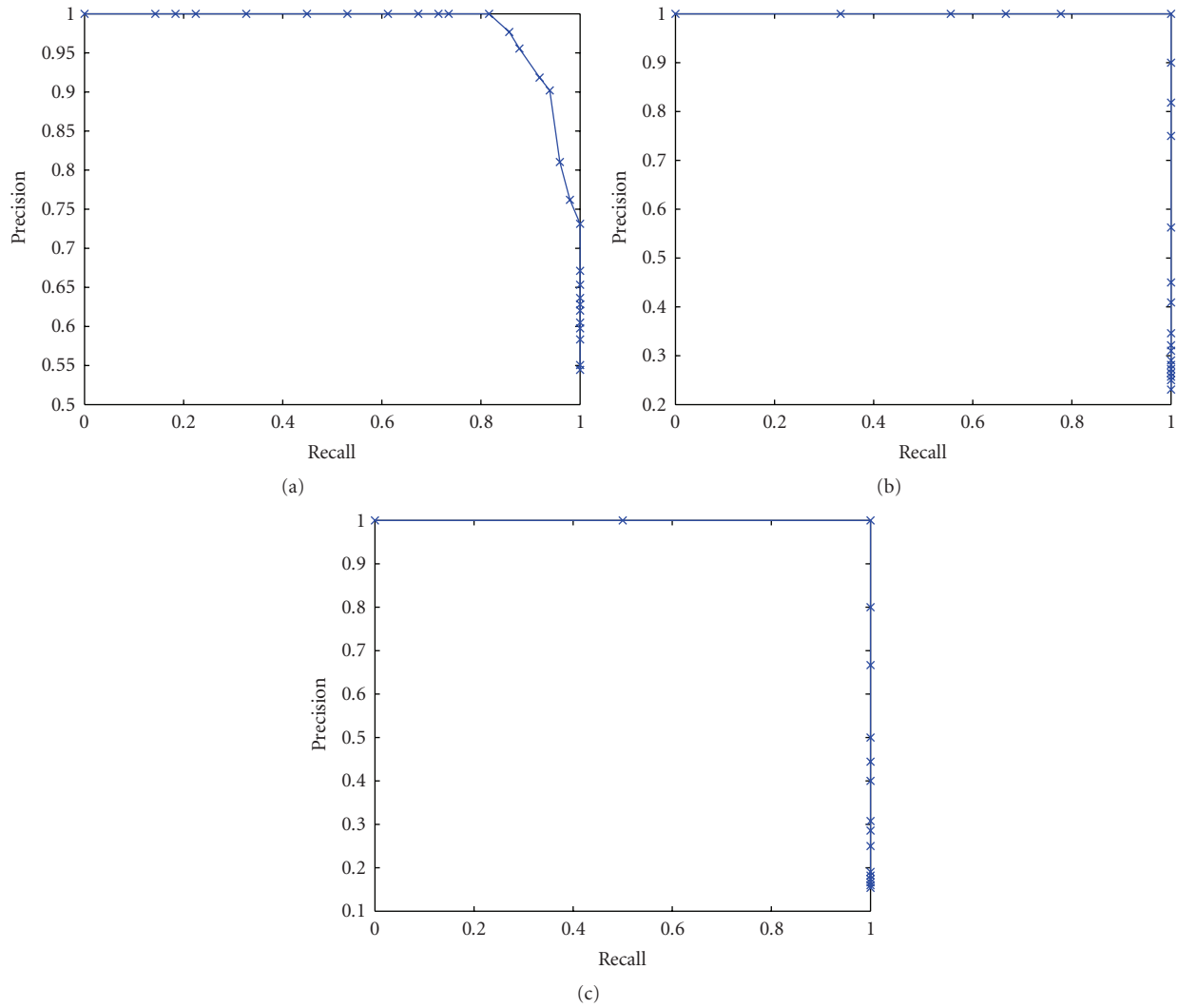


Figure 5: The recall versus precision rates for the detection of three different clusters of activities. (a) Walking activities (activities 1–5, 11, and 12 in Table 1). (b) Sitting activities (activities 6–9 in Table 1). (c) Brooming activities (activities 9 and 10 in Table 1).

applied different thresholds on the matrix and calculated the recall and precision values for each cluster. The first cluster contains the walking sequences along with jogging and blind walk (activities 1–5, 11, and 12 in Table 1). Figure 5(a) shows the recall versus precision values for this activity cluster; we can see from the figure that we are able to identify 90% of these activities with a precision up to 90%. The second cluster consists of three sitting sequences (activities 6–8 in Table 1), and the third cluster consists of the brooming sequences (activities 9 and 10 in Table 1). For both of these clusters the similarity values were quite separated to the extent that we were able to fully separate the positive and negative examples. This resulted in the recall versus precision curves as shown in Figures 5(b) and 5(c).

### 5.1.3. *View-invariant activity recognition*

In this part of the experiment, we consider the situation where we try to recognize activities when the training and testing video sequences are from different viewpoints. This is the most interesting part of the method as it demonstrates the strength of using 3D models for activity recognition. In our dataset, we had three sequences where the motion is not parallel to the image plane, two for jogging in a circle and one for brooming in a circle. We considered a portion of these sequences where the stick figure is not parallel to the camera. From each such video sequence, we computed the basis shapes. Each basis shape is rotated, based on an estimate of its pose, and transformed to the canonical plane (i.e., parallel to the image plane). The basis shapes before and after rotation are shown in Figure 6. The rotated basis shape is used to compute the similarity of this sequence with others, exactly as described above. Rows 14–18 of the similarity matrix show the recognition performance for this case. The jogging sequences are close to jogging in the canonical plane (column 11), followed by walking along the canonical plane (columns 1–6). For the broom sequence, it is closest to a brooming activity in the canonical plane (columns 9 and 10).

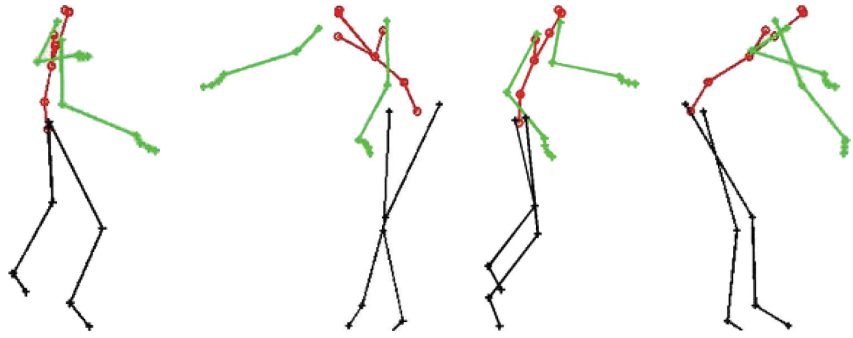


Figure 6: (a)-(b) Plot of the basis shapes for jogging and brooming when the viewing direction is different from the canonical one. (c)-(d) Plot of the rotated basis shapes.

The sitting and walking sequences (columns 17 and 18) of the test data are close to the sitting and walking sequences in the training data even though they were captured from different viewing directions.

### 5.2. Application in characterization of ground plane trajectories

Our second set of experiments was directed towards the special case of ground plane motion trajectories. The proposed algorithm was tested on a set of real trajectories, generated by applying a motion detection and tracking system [58] on the force protection surveillance system (FPSS) dataset provided by US Army Research Laboratory (ARL). These data sequences represent the monitoring of humans and vehicles moving around in a large parking lot. The normal activity in these sequences corresponds to a person moving into the parking lot and approaching his or her car, or stepping out of the car and moving out of the parking lot. We manually picked the trajectories corresponding to normal activities from the tracking results to assure stable tracking results in the training set.

In this experiment, we deal with a single normal activity. However, for more complicated scenes, the algorithm can handle multiple activities by first estimating the number of activities using the DI estimation procedure in Section 4 and then performing the following learning procedure for each activity.

#### 5.2.1. Time scaling

One of the major challenges in comparing activities is to remove the temporal variation in the way the activity is being executed. Several techniques were used to face this challenge as in [62], where the authors used dynamic time warping (DTW) [63] to learn the nature of time warps between different instants of each activity. This technique could have been used in our problem as a preprocessing stage for the trajectories to compensate for these variations before computing the nominal shape of each activity. However, the nature of the ground plane activities in our experiment did not require such sophisticated techniques; so we used a much simpler approach to be able to compare trajectories of different lengths (different number of samples $n$) and to explore the temporal effect. We adopt the multiresolution time scaling approach described below.

(i) Each trajectory is divided into segments of a common length $n$. We pick $n = 50$ frames in our experiment.

(ii) A multiscale technique is used for testing different combinations of segments, ranging from the finest scale (the line segments) to the coarsest scale (the whole trajectory). This technique gives the ability to evaluate each section of the trajectory along with the overall trajectory. An example of the different training sequences that can be obtained from a $3n$ trajectory is given in Table 2, where $Downsample_m$ denotes the process of keeping every $m$th sample and discarding the rest. We provide a representation of the segments in the form of an ordered pair $(i, j)$, where $i$ represents the scale of the segment and $j$ represents the order of this segment within the scale $i$.

An important property of this time scaling approach is that it captures the change in motion pattern between segments because of grouping of all possible combinations of adjacent segments. This can be helpful as the abrupt change in human motion pattern, like sudden running, is a change that is worthy of being singled out in surveillance applications.

#### 5.2.2. Ground plane recovery

This is the first step in our method. This calibration process needs to be done once for each camera, and the transformation matrix can then be used for all the subsequent sequences because of the stationary setup. The advantage of this method is that it does not need any ground truth information and can be performed using some features that are common in man-made environments.

As described before, the first stage recovers the affine parameters by identifying the vanishing line of the ground plane. This is done using two parallel lines as shown in Figure 7(a); the parallel lines are picked as the horizontal and vertical borders of a parking spot. Identifying the vanishing line is sufficient to recover the ground plane up to an affine transformation as shown in Figure 7(b).

Table 2: The different trajectory sequences generated from a three-segment trajectory.

| $x_1 \cdots x_n$ | $x_{n+1} \cdots x_{2n}$ | $x_{2n+1} \cdots x_{3n}$ |
|---|---|---|
| $y_1 \cdots y_n$ | $y_{n+1} \cdots y_{2n}$ | $y_{2n+1} \cdots y_{3n}$ |

| Scale | Segment representation | Trajectory points | Processing type |
|---|---|---|---|
| (1) | (1,1) | $x_1 : x_n$<br>$y_1 : y_n$ | *No processing*<br>*No processing* |
| | (1,2) | $x_{n+1} : x_{2n}$<br>$y_{n+1} : y_{2n}$ | *No processing*<br>*No processing* |
| | (1,3) | $x_{2n+1} : x_{3n}$<br>$y_{2n+1} : y_{3n}$ | *No processing*<br>*No processing* |
| (2) | (2,1) | $x_1 : x_{2n}$<br>$y_1 : y_{2n}$ | $Downsample_2$<br>$Downsample_2$ |
| | (2,2) | $x_{n+1} : x_{3n}$<br>$y_{n+1} : y_{3n}$ | $Downsample_2$<br>$Downsample_2$ |
| (3) | (3,1) | $x_1 : x_{3n}$<br>$y_1 : y_{3n}$ | $Downsample_3$<br>$Downsample_3$ |

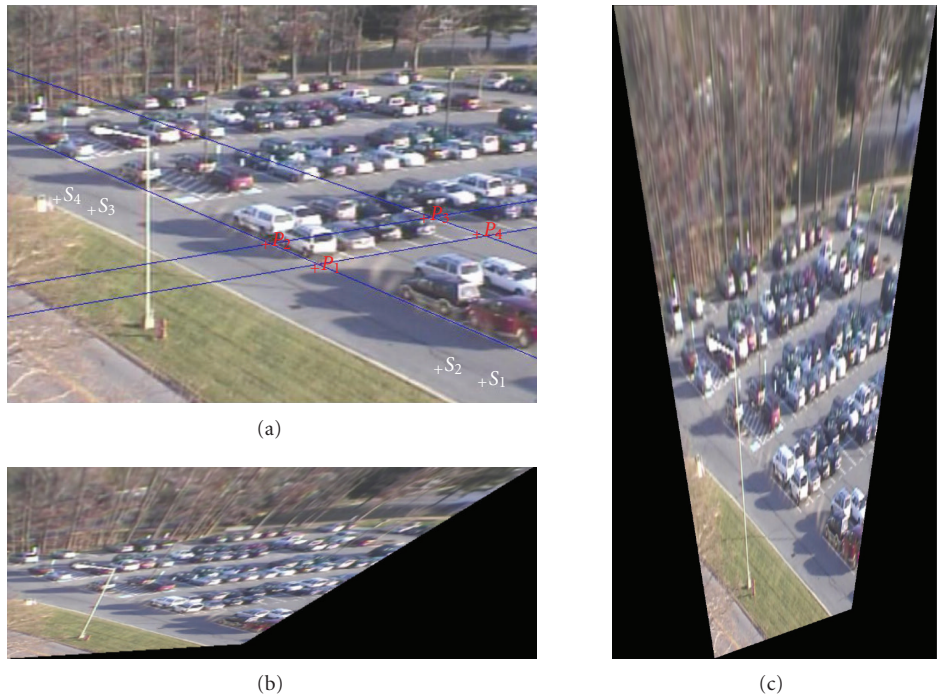


(a) (b) (c)

Figure 7: The recovery of the ground plane. (a) The original image frame with the features used in the recovery process. (b) The affine rectified image. (c) The metric rectified image.

The second stage is to recover the ground plane up to a metric transformation, which is achieved using two affine invariant properties. The recovery result is shown in Figure 7(c). In our experiment, we used the right angle between the vertical and horizontal borders of parking space and the equal length of the tire spans of a tracked truck across frame as shown by the white points $(S_1, S_2)$ and $(S_3, S_4)$ in Figure 7(a).

### 5.2.3. *Learning the trajectories*

For learning the normal activity trajectory, we used a training dataset containing the tracking results for 17 objects of different track lengths. The normal activity in such data corresponds to a person entering the parking lot and moving towards a car, or a person leaving the parking lot. The trajectories were first smoothed using a five-point moving averaging to remove tracking errors, and then they were used to generate track segments of 50-point length as described earlier, resulting in 60 learning segments. Figure 8(a) shows the image plane trajectories used in the learning process, and each of the red points represents the center of the bounding box of an object in a certain frame.

This set of trajectories is used to determine the range of the NMSE in the case of a normal activity trajectory. Figure 8(b) shows the NMSE values for the segments of the training set sequence.

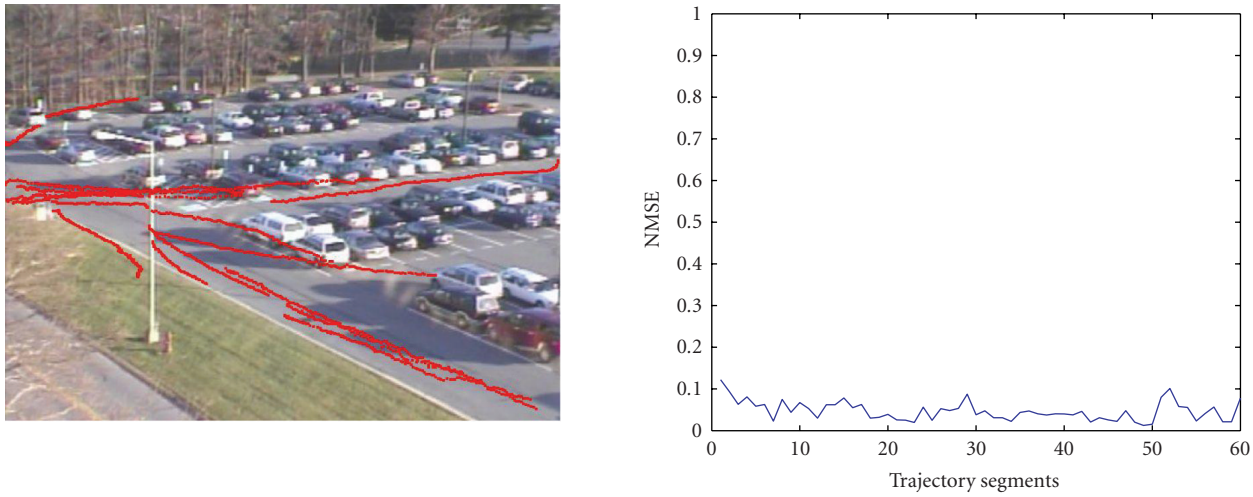


(a) (b)

Figure 8: (a) The normal trajectories and (b) the associated normalized mean square error (NMSE) values.

NMSE(1, 1) = 0.0225

NMSE(1, 2) = 0.0296
NMSE(2, 1) = 0.0146

NMSE(1, 3) = 0.3357
NMSE(2, 2) = 0.1809
NMSE(3, 1) = 0.1123

(a) (b) (c)

Figure 9: The first abnormal test scenario. A person stops moving at a point on his route. We see the increase in the normalized mean square error (NMSE) values when he/she stops, resulting in a deviation from the normal trajectory.¡?layout cmd=”vspace” calue=”2”?¿

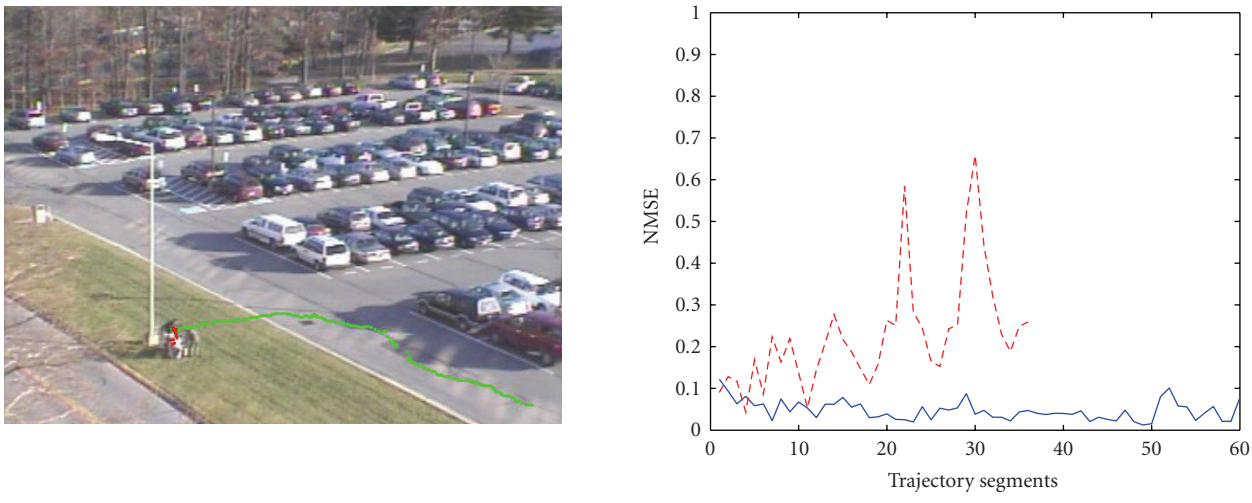


(a) (b)

Figure 10: The second testing scenario. (a) A group of people on a path towards a box. (b) The increase in the NMSE with time as the abnormal scenario is being performed.

#### 5.2.4. Testing trajectories for anomalies

*First abnormal scenario*

This testing sequence represents a human moving in the parking lot and then stopping in the same location for some time. The first part of the trajectory, which lasts for 100 frames (two segments), is a normal activity trajectory, but the third segment represents an abnormal act. This could be a situation of interest in surveillance scenario. Figure 9 shows the different segments of the object trajectory, along with the NMSE associated with each new segment. We see that as the object stops moving in the third segment, the NMSE values rise to indicate a possible drift of the object trajectory from the normal trajectory.

*Second abnormal scenario*

In this abnormal scenario, several tracked humans drift from their path into the grass area surrounding the parking lot, stop there to lift a large box, and then move the box. Figure 10(a) shows the object trajectory. Figure 10(b) shows a plot of the NMSE of all the segments, in red, with respect to the normal trajectory NMSE, in blue. It can be verified from the figure that the trajectory was changing from normal to abnormal one in the last three or four segments, which caused the NMSE of the global trajectory to rise.

## 6. CONCLUSIONS

In this paper, we have presented a framework for using 3D deformable shape models for activity modeling and representation. This has the potential to provide invariance to viewpoint and more detailed modeling of illumination effects. The 3D shape is estimated from the motion trajectories of the points participating in the activity under a weak perspective camera projection model. Each activity is represented using a linear combination of a set of 3D basis shapes. We presented a theory for estimating the number of basis shapes, based on the DI of the 3D deformable shape. We also explored the special case of ground plane motion trajectories, which often occurs in surveillance applications, and provided a framework for using our proposed approach for detecting anomalies in this case. We presented results showing the effectiveness of our 3D model in representing human activity for recognition and performing ground plane activity modeling and anomaly detection. The main challenge in this framework will be in developing representations that are robust to errors in 3D model estimation. Also, machine learning approaches that take particular advantage of the availability of 3D models will be an interesting area of future research.

## ACKNOWLEDGMENTS

M. Abdelkader and R. Chellappa were partially supported by the Advanced Sensors Consortium sponsored by the US Army Research Laboratory under the Collaborative Technology Alliance Program, Cooperative Agreement DAAD19-01-2-0008. A. K. Roy-Chowdhury was partially supported by NSF Grant IIS-0712253 while working on this paper. The authors thank Dr. Alex Chan and Dr. Nasser Nasrabadi for providing ARL data and helpful discussions.

## REFERENCES

[1] D. Kendall, D. Barden, T. Carne, and H. Le, *Shape and Shape Theory*, John Wiley & Sons, New York, NY, USA, 1999.

[2] I. Dryden and K. Mardia, *Statistical Shape Analysis*, John Wiley & Sons, New York, NY, USA, 1998.

[3] T. Cootes, C. Taylor, D. Cooper, and J. Graham, "Active shape models - their training and application," Computer Vision and Image Understanding , vol. 61, no. 1, pp. 38–59, 1995.

[4] W. Mio and A. Srivastava, "Elastic-string models for representation and analysis of planar shapes," in *Proceedings of the IEEE Computer Society Conference on Computer Vision and Pattern Recognition (CVPR '04)*, vol. 2, pp. 10–15, Washington, DC, USA, June-July 2004.

[5] T. B. Sebastian, P. N. Klein, and B. B. Kimia, "Recognition of shapes by editing their shock graphs," IEEE Transactions on Pattern Analysis and Machine Intelligence , vol. 26, no. 5, pp. 550–571, 2004.

[6] A. Srivastava, S. H. Joshi, W. Mio, and X. Liu, "Statistical shape analysis: clustering, learning, and testing," IEEE Transactions on Pattern Analysis and Machine Intelligence , vol. 27, no. 4, pp. 590–602, 2005.

[7] L. Torresani, D. Yang, E. Alexander, and C. Bregler, "Tracking and modeling non-rigid objects with rank constraints," in *Proceedings of the IEEE Computer Society Conference on Computer Vision and Pattern Recognition (CVPR '01)*, vol. 1, pp. 493–500, Kauai, Hawaii, USA, December 2001.

[8] M. Brand, "Morphable 3D models from video," in *Proceedings of the IEEE Computer Society Conference on Computer Vision and Pattern Recognition (CVPR '01)*, vol. 2, pp. 456–463, Kauai, Hawaii, USA, December 2001.

[9] J. Xiao, J. Chai, and T. Kanade, "A closed-form solution to non-rigid shape and motion recovery," in *Proceedings of the 8th European Conference on Computer Vision (ECCV '04)*, vol. 3024, pp. 573–587, Prague, Czech Republic, May 2004.

[10] M. Brand, "A direct method for 3D factorization of nonrigid motion observed in 2D," in *Proceedings of the IEEE Computer Society Conference on Computer Vision and Pattern Recognition (CVPR '05)*, vol. 2, pp. 122–128, San Diego, Calif, USA, June 2005.

[11] Y. Sheikh, M. Sheikh, and M. Shah, "Exploring the space of a human actionin," in *Proceedings of the 10th IEEE International Conference on Computer Vision (ICCV '05)*, vol. 1, pp. 144–149, Beijing, China, October 2005.

[12] A. Veeraraghavan, A. K. Roy-Chowdhury, and R. Chellappa, "Matching shape sequences in video with applications in human movement analysis," IEEE Transactions on Pattern Analysis and Machine Intelligence , vol. 27, no. 12, pp. 1896–1909, 2005.

[13] N. Vaswani, A. K. Roy-Chowdhury, and R. Chellappa, ""Shape activity": a continous-state HMM for moving/deforming shapes with application to abnormal activity detection," IEEE Transactions on Image Processing , vol. 14, no. 10, pp. 1603–1616, 2005.

[14] A. K. Roy-Chowdhury and R. Chellappa, "Factorization approach for event recognition," in *Proceedings of CVPR Event Mining Workshop*, Madison, Wis, USA, June 2003.

[15] A. K. Roy-Chowdhury, "A measure of deformability of shapes, with applications to human motion analysis," in *Proceedings*

*of the IEEE Computer Society Conference on Computer Vision and Pattern Recognition (CVPR '05)*, vol. 1, pp. 398–404, San Diego, Calif, USA, June 2005.

[16] A. K. Roy-Chowdhury, "Towards a measure of deformability of shape sequences," Pattern Recognition Letters , vol. 28, no. 15, pp. 2164–2172, 2007.

[17] S. Tsuji, A. Morizono, and S. Kuroda, "Understanding a simple cartoon film by a computer vision system," in *Proceedings of the 5th International Joint Conference on Artificial Intelligence (IJCAI '77)*, pp. 609–610, Cambridge, Mass, USA, August 1977.

[18] B. Neumann and H. Novak, "Event models for recognition and natural language descriptions of events in real-world image sequences," in *Proceedings of the 8th International Joint Conference on Artificial Intelligence (IJCAI '83)*, pp. 724–726, Karlsruhe, Germany, August 1983.

[19] H. Nagel, "From image sequences towards conceptual descriptions," Image and Vision Computing , vol. 6, no. 2, pp. 59–74, 1988.

[20] Y. Kuniyoshi and H. Inoue, "Qualitative recognition of ongoing human action sequences," in *Proceedings of the 13th International Joint Conference on Artificial Intelligence (IJCAI '93)*, pp. 1600–1609, Chambéry, France, August-September 1993.

[21] C. Dousson, P. Gabarit, and M. Ghallab, "Situation recognition: representation and algorithms," in *Proceedings of the 13th International Joint Conference on Artificial Intelligence (IJCAI '93)*, pp. 166–172, Chambéry, France, August-September 1993.

[22] H. Buxton and S. Gong, "Visual surveillance in a dynamic and uncertain world," Artificial Intelligence , vol. 78, no. 1-2, pp. 431–459, 1995.

[23] J. Davis and A. Bobick, "Representation and recognition of human movement using temporal templates," in *Proceedings of the IEEE Computer Society Conference on Computer Vision and Pattern Recognition (CVPR '97)*, pp. 928–934, San Juan, Puerto Rico, USA, June 1997.

[24] B. F. Bremond and M. Thonnat, "Analysis of human activities described by image sequences," in *Proceedings of the 20th International Florida Artificial Intelligence Research International Symposium (FLAIRS '97)*, Daytona, Fla, USA, May 1997.

[25] N. Rota and M. Thonnat, "Activity recognition from video sequence using declarative models," in *Proceedings of the 14th European Conference on Artificial Intelligence (ECAI '00)*, pp. 673–680, Berlin, Germany, August 2000.

[26] V. Vu, F. Bremond, and M. Thonnat, "Automatic video interpretation: a recognition algorithm for temporal scenarios based on pre-compiled scenario models," in *Proceedings of IEEE International Conference on Computer Vision Systems (ICCV '03)*, pp. 523–533, Graz, Austria, April 2003.

[27] C. Castel, L. Chaudron, and C. Tessier, "What is going on? A high-level interpretation of a sequence of images," in *Proceedings of the Workshop on Conceptual Descriptions from Images (ECCV '96)*, Cambridge, UK, April 1996.

[28] T. Starner and A. Pentland, "Visual recognition of American sign language using hidden Markov models," in *Proceedings of the International Workshop on Face and Gesture Recognition*, 1995.

[29] A. Wilson and A. Bobick, "Recognition and interpretation of parametric gesture," in *Proceedings of the IEEE 6th International Conference on Computer Vision (ICCV '98)*, pp. 329–336, Bombay, India, January 1998.

[30] W. Grimson, C. Stauffer, R. Romano, and L. Lee, "Using adaptive tracking to classify and monitor activities in a site," in *Proceedings of the IEEE Computer Society Conference on Computer Vision and Pattern Recognition (CVPR '98)*, pp. 22–29, Santa Barbara, Calif, USA, June 1998.

[31] J. Pearl, *Probabilistic Reasoning in Intelligent Systems*, Morgan Kaufmann, San Francisco, Calif, USA, 1988.

[32] S. Intille and A. Bobick, "A framework for recognizing multi-agent action from visual evidence," in *Proceedings of the National Conference on Artificial Intelligence (AAAI '99)*, pp. 518–525, Orlando, Fla, USA, July 1999.

[33] P. Remagnini, T. Tan, and K. Baker, "Agent-oriented annotation in model based visual surveillance," in *Proceedings of the International Conference on Computer Vision (ICCV '98)*, pp. 857–862, Bombay, India, January 1998.

[34] G. Shaffer, *A Mathematical Theory of Evidence*, Princeton University Press, Princeton, NJ, USA, 1976.

[35] D. Ayers and R. Chellappa, "Scenario recognition from video using a hierarchy of dynamic belief networks," in *Proceedings of the 15th International Conference on Pattern Recognition (ICPR '00)*, vol. 1, pp. 835–838, Barcelona, Spain, September 2000.

[36] T. Huang, D. Koller, and J. Malik, "Automatic symbolic traffic scene analysis using belief networks," in *Proceedings of the 12th National Conference on Artificial Intelligence (AAAI '94)*, pp. 966–972, Seattle, Wash, USA, July 1994.

[37] S. Hongeng and R. Nevatia, "Multi-agent event recognition," in *Proceedings of the 8th IEEE International Conference on Computer Vision (ICCV '01)*, pp. 84–91, Vancouver, BC, Canada, July 2001.

[38] G. Johansson, "Visual perception of biological motion and a model for its analysis," Perception and Psychophysics , vol. 14, no. 2, pp. 201–211, 1973.

[39] E. Muybridge, *The Human Figure in Motion*, Dover, New York, NY, USA, 1901.

[40] G. Harris and P. Smith, Eds., *Human Motion Analysis: Current Applications and Future Directions*, IEEE Press, Piscataway, NJ, USA, 1996.

[41] D. Gavrila, "The visual analysis of human movement: a survey," Computer Vision and Image Understanding , vol. 73, no. 1, pp. 82–98, 1999.

[42] W. Hu, T. Tan, L. Wang, and S. Maybank, "A survey on visual surveillance of object motion and behaviors," IEEE Transactions on Systems, Man and Cybernetics Part C: Applications and Reviews , vol. 34, no. 3, pp. 334–352, 2004.

[43] N. Vaswani, A. K. Roy-Chowdhury, and R. Chellappa, "Activity recognition using the dynamics of the configuration of interacting objects," in *Proceedings of the IEEE Computer Society Conference on Computer Vision and Pattern Recognition (CVPR '03)*, vol. 2, pp. 633–640, Madison, Wis, USA, June 2003.

[44] A. Veeraraghavan, A. K. Roy-Chowdhury, and R. Chellappa, "Role of shape and kinematics in human movement analysis," in *Proceedings of the IEEE Computer Society Conference on Computer Vision and Pattern Recognition (CVPR '04)*, vol. 1, pp. 730–737, Washington, DC, USA, June-July 2004.

[45] L. Campbell and A. Bobick, "Recognition of human body motion using phase space constraints," in *Proceedings of the IEEE 5th International Conference on Computer Vision (ICCV '95)*, pp. 624–630, Cambridge, Mass, USA, June 1995.

[46] C. Rao, A. Yilmaz, and M. Shah, "View-invariant representation and recognition of actions," International Journal of Computer Vision , vol. 50, no. 2, pp. 203–226, 2002.

[47] V. Parameswaran and R. Chellappa, "View invariants for human action recognition," in *Proceedings of the IEEE Computer Society Conference on Computer Vision and Pattern*

*Recognition (CVPR '03)*, vol. 2, pp. 613–619, Madison, Wis, USA, June 2003.

[48] N. Johnson and D. Hogg, "Learning the distribution of object trajectories for event recognition," Image and Vision Computing , vol. 14, no. 8, pp. 609–615, 1996.

[49] J. Owens and A. Hunter, "Application of the self-organizing map to trajectory classification," in *Proceedings of the IEEE International Workshop Visual Surveillance*, pp. 77–83, Dublin, Ireland, July 2000.

[50] W. Chen and S. F. Chang, "Motion trajectory matching of video objects," in *Storage and Retrieval for Media Databases*, vol. 3972 of *Proceedings of SPIE*, pp. 544–553, San Jose, Calif, USA, January 2000.

[51] L. Torresani and C. Bregler, "Space-time tracking," in *Proceedings of the 7th European Conference on Computer Vision (ECCV '02)*, Copenhagen, Denmark, May-June 2002.

[52] P. J. Phillips, S. Sarkar, I. Robledo, P. Grother, and K. Bowyer, "The gait identification challenge problem: data sets and baseline algorithm," in *Proceedings of the 16th International Conference on Pattern Recognition (ICPR '02)*, vol. 16, pp. 385–388, Quebec City, Canada, August 2002.

[53] C. Tomasi and T. Kanade, "Shape and motion from image streams under orthography: a factorization method," International Journal of Computer Vision , vol. 9, no. 2, pp. 137–154, 1992.

[54] Z. Zhang, "A flexible new technique for camera calibration," IEEE Transactions on Pattern Analysis and Machine Intelligence , vol. 22, no. 11, pp. 1330–1334, 2000.

[55] R. Tsai, "A versatile camera calibration technique for high-accuracy 3D machine vision metrology using off-the-shelf TV cameras and lenses," IEEE Journal of [legacy, pre - 1988] on Robotics and Automation , vol. 3, no. 4, pp. 323–344, 1987.

[56] D. Liebowitz and A. Zisserman, "Metric rectification for perspective images of planes," in *Proceedings of the IEEE Computer Society Conference on Computer Vision and Pattern Recognition (CVPR '98)*, pp. 482–488, Santa Barbara, Calif, USA, June 1998.

[57] R. Hartley and A. Zisserman, *Multiple View Geometry in Computer Vision*, Cambridge University Press, New York, NY, USA, 2000.

[58] M. F. Abdelkader, R. Chellappa, Q. Zheng, and A. L. Chan, "Integrated motion detection and tracking for visual surveillance," in *Proceedings of the 4th IEEE International Conference on Computer Vision Systems (ICVS '06)*, p. 28, New York, NY, USA, January 2006.

[59] Cornegie mellon university graphics lab motion capture database, http://mocap.cs.cmu.edu/ .

[60] A. Kale, A. Sundaresan, and A. Rajagopalan, "Identification of humans using gait," IEEE Transactions on Image Processing , vol. 13, no. 9, pp. 1163–1173, 2004.

[61] R. Tanawongsuwan and A. Bobick, "Modelling the effects of walking speed on appearance-based gait recognition," in *Proceedings of the IEEE Computer Society Conference on Computer Vision and Pattern Recognition (CVPR '04)*, vol. 2, pp. 783–790, Washington, DC, USA, June-July 2004.

[62] A. Veeraraghavan, R. Chellappa, and A. K. Roy-Chowdhury, "The function space of an activity," in *Proceedings of the IEEE Computer Society Conference on Computer Vision and Pattern Recognition (CVPR '06)*, pp. 959–968, Washington, DC, USA, 2006.

[63] L. Rabiner and B.-H. Juang, *Fundamentals of Speech Recognition*, Prentice-Hall, Upper Saddle River, NJ, USA, 1993.